Journal of Molecular Structure 981 (2010) 139–145

Contents lists available at ScienceDirect

Journal of Molecular Structure

journal homepage: www.elsevier.com/locate/molstruc

Syntheses, crystal structures, and magnetic properties of two molecular materials by self-assembly of bis(maleonitriledithiolato)nickelate monoanion and substituted benzyltriphenylphosphinium

Xing Chen [a], Hai-Lian Zhou [a], Jing-Hua Lin [a], Qian Huang [a], Hong-Rong Zuo [a], Jia-Rong Zhou [a], Chun-Lin Ni [a,*], Xue-Lei Hu [b]

[a] Department of Applied Chemistry, Institute of Biomaterial, College of Science, South China Agricultural University, 510642 Guangzhou, PR China
[b] School of Chemical Engineering and Pharmacy, Wuhan Institute of Technology, 430073 Wuhan, PR China

ARTICLE INFO

Article history:
Received 9 April 2010
Received in revised form 26 July 2010
Accepted 27 July 2010
Available online 3 August 2010

Keywords:
3-Substituted benzyltriphenylphosphinium
Bis(maleonitriledithiolato)nicklelate monoanion
Crystal structures
Magnetic properties
Spin-gap transition

ABSTRACT

Two molecular materials, [3RBzTPP][Ni(mnt)$_2$] (mnt^{2-} = maleonitriledithiolate, [3RBzTPP]$^+$ = 3-R-benzyltriphenylphosphinium, R = CN(**1**), F(**2**)), have been investigated and characterized by elemental analyses, IR, UV spectroscopy, X-ray diffraction and magnetic susceptibility measurements. The [Ni(mnt)$_2$]$^-$ anions of **1** and **2** stack into a column through the Ni···S or/and S···S interactions with a Ni···S distance of 3.765 Å for **1** and with the Ni···S and S···S distances of 3.654 Å and 3.681 Å for **2**. The weak C—H···N, C—H···F hydrogen bonds and π···π stacking interactions result in the forming of a 3D network structure. Magnetic susceptibility measurements in the temperature range 2–300 K show that **1** shows an antiferromagnetic coupling behavior with $\theta = -9.3$ K, and **2** exhibits a spin-gap transition with $\Delta/k_b = 945.0$ K around 217 K.

1. Introduction

Duo to their ability to assemble in the solid state with the non-covalent bond such as short S···S, M···S (M = Ni, Cu or Pd), C—H···X (X = N, S, F, Cl, Br, O, etc.) or π···π stacking interactions [1–5], transition metal complexes of the dithiolenes have been widely used as functional materials for a number of applications, including conducting and magnetic materials dyes [6], non-linear optical materials [7–9], and electro-active substrates in olefin separation methods [10]. The stacking mode of the molecular of these materials can be tuned through changing the metal [11] ions or modification of the organic dithiolene ligands [12–15], and the counter-cations [16,17]. In this regard, the spin molecular system based on [M(mnt)$_2$]$^-$ (M = Ni, Pd or Pt) had been synthesised and proved to be good building block to construct molecular materials which exhibit an attractive planar configuration and the highly sensitive magnetic coupling [18–21]. The work in our laboratory is to find more suitable multifunctional organic cations to tune the crystal stacking structure of the molecular solids containing the [M(mnt)$_2$]$^-$ anion, and obtain some new molecular magnetic materials. Recently, we have been investigating the syntheses, crystal structures, weak interactions and magnetic properties of the ion-pair complexes by self-assembly of the [Ni(mnt)$_2$]$^-$ anion and substituted benzyltriphenylphosphinium cations such as [BzTPP]$^+$ [22], [oClBzTPP]$^+$ [23], [4CNBzTPP]$^+$ and [4ClBzTPP]$^+$ [24]. In order to extend our studies, here we have used [3RBzTPP]$^+$ (R = CN, F) as counter-cations to obtain two new ion-pair complexes [3CNBzTPP][Ni(mnt)$_2$] (**1**) and [3FBzTPP][Ni(mnt)$_2$] (**2**). As a result, when we changed the R group of 3-position on the phenyl ring of the benzyl group from CN to F, the crystal system, the stacking pattern of the anions and cations, the overlapping mode of the anions, and the magnetic properties of the molecular materials have significantly been changed.

2. Experimental

All reagents and chemicals were purchased from commercial sources and were used as received. Disodium maleonitriledithiolate (Na$_2$mnt) was synthesized follow the published procedure [25]. 3-cyanobenzyltriphenylphosphinium bromide ([3CNBzTPP]Br) and 3-fluorobenzyltriphenylphosphinium bromide ([3FBzTPP]Br) were prepared by literature methods [26]. A similar method for preparing [4CNBzTPP][Ni(mnt)$_2$] was used to prepare [3CNBzTPP][Ni(mnt)$_2$] and [3FBzTPP][Ni(mnt)$_2$] [24].

* Corresponding author. Tel.: +86 20 85282568; fax: +86 20 85282366.
E-mail address: niclchem@scau.edu.cn (C.-L. Ni).

0022-2860/$ - see front matter © 2010 Elsevier B.V. All rights reserved.
doi:10.1016/j.molstruc.2010.07.042

2.1. Synthesis of [3CNBzTPP][Ni(mnt)$_2$](**1**)

A methanol solution (10 mL) of Na_2mnt (370 mg, 1 mmol) was added to a methanol solution (10 mL) of $NiCl_2{\cdot}6H_2O$ (240 mg, 1 mmol) while stirring, and the mixture was continuously stirred for 45 min at room temperature. The equal amount of I_2 was dissolved in 30 mL methanol, and added to the above solution at one portion, the mixture was warmed at 45 centigrade for 15 min, then 30 mL methanol solution of [3CNBzTPP]Br (505 mg, 1.1 mmol) was dropped to the mixture slowly, cooled down after another 1.5 h when all the [3CNBzTPP]Br was added. The product was collected via filtration, wasted with cool methanol and diethyl ether, and air-dried. Yield: 490 mg, 68%. *Anal.* Calc. for $C_{34}H_{21}N_5NiPS_4$: C, 56.92; H, 2.95; N, 9.76%; Found: C, 56.97; H, 3.08; N, 9.65%. IR spectrum (cm^{-1}): ν(CN), 2235 w, 2208 s; ν(C=C) of mnt^{2-}, 1439 s. UV spectrum (nm): 288, 269, 311.

2.2. Synthesis of [FBzTPP][Ni(mnt)$_2$](**2**)

Compound **2** was prepared by the same processing as that of **1**. Yield: 482 mg, 67%. *Anal.* Calc. for $C_{33}H_{21}N_4NiFPS_4$ (**2**): C, 55.79; H, 2.98; N, 7.89%. Found: C, 55.85; H, 3.10; N, 7.83%. IR (KBr, cm^{-1}): IR spectrum (cm^{-1}): ν(CN), 2207 s; ν(C=C) of mnt^{2-}, 1438 s. ν(C—F), 1111 s. UV spectrum (nm): 249, 287, 269, 312.

The black single-crystals suitable for the X-ray structure analyses were obtained by slowly cooling the solution of **1** and **2** in MeCN about 2 days at 5° below 0 °C.

2.3. Instrumental procedures

Elemental analyses of C, H, and N were run on a Model 240 Perkin Elmer CHN instrument. UV–Vis absorption spectrum in MeCN (1.0×10^{-6} mol L^{-1}) in the region of 230–700 nm was obtained by Shimadzu UV-2500 spectrophotometer. IR spectra were recorded from KBr pellets on a Nicolet FT-IR spectrophotometer in 4000–400 cm^{-1} regions. Magnetic susceptibility measurements were performed with a Quantum Design instrument with a super-conducting quantum interference device (SQUID) magnetometer working in the temperature range of 2–300 K under an external magnetic filed of 2000 Oe. Diamagnetic corrections were estimated from Pascal's tables.

Table 1
Crystal data and structure refinement for **1** and **2**.

Compounds	**1**	**2**
Empirical formula	$C_{34}H_{21}N_5NiPS_4$	$C_{33}H_{21}N_4NiFPS_4$
Formula weight	717.48	710.46
T (K)	291(2)	291(2)
Wavelength	0.71073 Å	0.71073 Å
Crystal system	Monoclinic	Triclinic
Space group	$P2_1/n$	P-1
a (Å)	8.8772(13)	8.5367(11)
b (Å)	17.460(3)	13.6664(18)
c (Å)	21.894(3)	14.9912(19)
α (°)	90	99.786(2)
β (°)	93.737(2)	103.369(2)
γ (°)	90	100.488(2)
Volume (Å^3)	3386.3(9)	1631.5(4)
Z	4	2
Density (calculated) (mg/m^3)	1.407	1.446
Absorption coefficient (mm^{-1})	0.899	0.935
F(0 0 0)	1468	726
Crystal size (mm^3)	0.11 × 0.15 × 0.21	0.07 × 0.12 × 0.19
Reflections collected	23,789	11,767
Independent reflections	5968(R_{int} = 0.051)	5689 (R_{int} = 0.028)
Data/restraints/parameters	5968/0/409	5689/0/397
Goodness of fit on F^2	1.013	1.014
Final R indices [$I > 2\sigma(I)$]	$R1$ = 0.0388	$R1$ = 0.0494
	$wR2$ = 0.0910	$wR2$ = 0.1448
Final R indices (all data)	$R1$ = 0.0661	$R1$ = 0.0680
	$wR2$ = 0.1114	$wR2$ = 0.1697

2.4. Crystal structure determination

The X-ray single-crystal data for **1** and **2** were measured on a Bruker Smart APEX CCD area detector. Graphite-monochromated Mo Kα radiation (λ = 0.71073 Å) and the ω-scan technique were used to collect the data sets. The crystallographic data, the conditions for the intensity data collection, and some features of the structure refinements are listed in Table 1. The structures were solved by direct methods and refined by full-matrix least-squares methods on F^2 employing the Bruker's SHELXTL [27]. All non-hydrogen atoms were refined with anisotropically. The hydrogen atoms were located on calculated positions, and their isotropic displacement factors were set to 1.2 times the value of the equivalent isotropic displacement parameters of the corresponding parent atoms. Significant bond parameters for **1** and **2** are given in Tables 2 and 3.

3. Results and discussion

3.1. Description of crystal structures

The X-ray study of [3CNBzTPP][Ni(mnt)$_2$](**1**) reveals that it crystallizes in monoclinic lattice with $P2_1/n$ group, and a labeled ORTEP plot of the asymmetric unit of **1** is shown in Fig. 1. The structure

Table 2
Selected bond lengths and bond angles for **1**.

Bond length (Å)			
Ni(1)—S(1)	2.148(1)	P(1)—C(15)	1.817(3)
Ni(1)—S(2)	2.148(1)	P(1)—C(21)	1.799(3)
Ni(2)—S(3)	2.135(1)	P(1)—C(27)	1.800(3)
Ni(2)—S(4)	2.142(1)	P(1)—C(33)	1.786(3)
S(1)—C(2)	1.722(3)	N(1)—C(1)	1.137(5)
S(2)—C(4)	1.727(3)	N(2)—C(3)	1.139(5)
S(3)—C(6)	1.722(4)	N(3)—C(5)	1.133(5)
S(4)—C(8)	1.720(4)	N(4)—C(7)	1.135(7)
N(5)—C(34)	1.142(6)		
Bond angles (°)			
S(1)—Ni(1)—S(2)	87.16(3)	Ni(2)—S(4)—C(8)	103.77(12)
S(1)—Ni(1)—S(2)#1	92.84(3)	C(15)—P(1)—C(21)	108.58(14)
S(3)—Ni(2)—S(4)	87.99(4)	C(15)—P(1)—C(27)	111.65(14)
S(3)—Ni(2)—S(4)#2	92.01(4)	C(15)—P(1)—C(33)	106.83(13)
Ni(1)—S(1)—C(2)	102.81(11)	C(21)—P(1)—C(27)	109.24(13)
Ni(1)—S(2)—C(4)	102.96(11)	C(21)—P(1)—C(33)	110.23(14)
Ni(2)—S(3)—C(6)	103.95(12)	C(27)—P(1)—C(33)	110.28(14)

Symmetry transformations used to generate equivalent atoms: #1 = $-x$, $-y$ + 2, $-z$; #2 = $-x$ + 1, $-y$, $-z$.

Table 3
Selected bond lengths and bond angles for **2**.

Bond length (Å)			
Ni(1)—S(1)	2.150(1)	P(1)—C(15)	1.823(5)
Ni(1)—S(2)	2.146(1)	P(1)—C(21)	1.793(4)
Ni(1)—S(3)	2.152(1)	P(1)—C(27)	1.796(4)
Ni(1)—S(4)	2.144(1)	P(1)—C(33)	1.795(4)
S(1)—C(2)	1.723(5)	N(1)—C(1)	1.138(7)
S(2)—C(3)	1.723(5)	N(2)—C(4)	1.139(8)
S(3)—C(6)	1.716(5)	N(3)—C(5)	1.129(8)
S(4)—C(7)	1.720(4)	N(4)—C(8)	1.133(7)
Bond angles (°)			
S(1)—Ni(1)—S(2)	92.72(5)	Ni(1)—S(4)—C(7)	103.35(16)
S(1)—Ni(1)—S(3)	178.15(6)	C(15)—P(1)—C(21)	108.3(2)
S(1)—Ni(1)—S(4)	87.61(5)	C(15)—P(1)—C(27)	109.1(2)
S(2)—Ni(1)—S(3)	87.35(5)	C(15)—P(1)—C(33)	110.1(2)
S(2)—Ni(1)—S(4)	179.67(5)	C(21)—P(1)—C(27)	109.5(2)
S(3)—Ni(1)—S(4)	92.32(5)	C(21)—P(1)—C(33)	110.8(2)
Ni(1)—S(1)—C(2)	103.16(16)	C(27)—P(1)—C(33)	109.2(2)
Ni(1)—S(3)—C(6)	103.43(16)	F(1)—C(10)—C(11)	116.3(6)

Symmetry transformations used to generate equivalent atoms: #1: $-x$, $-y$, $-z$ + 1.

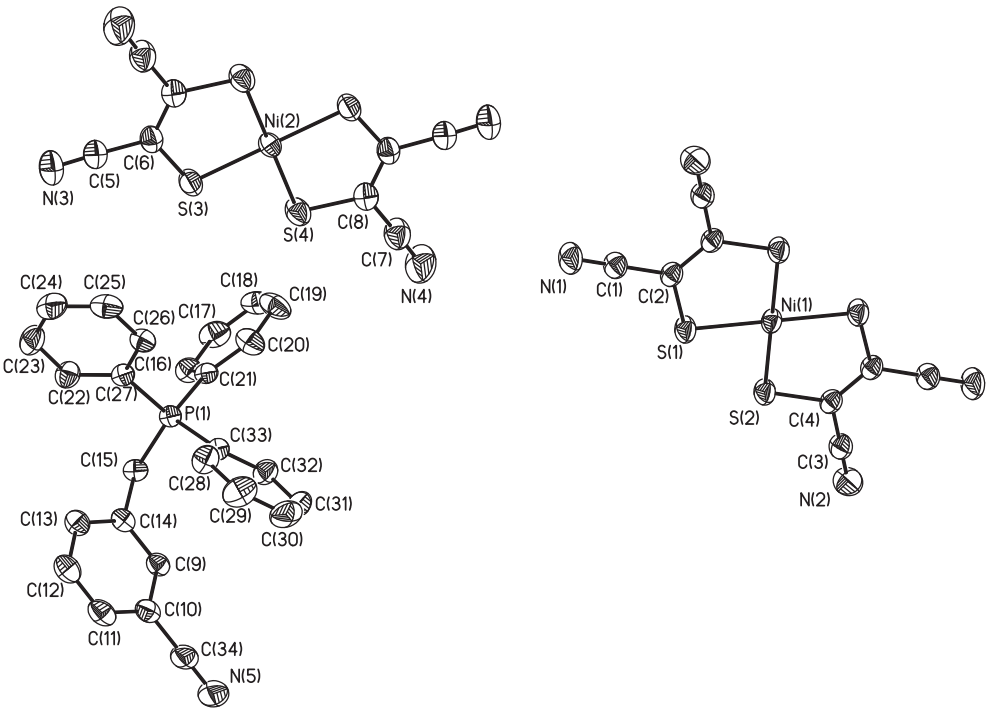

Fig. 1. ORTEP plot (30% probability ellipsoids) showing the molecule structure of **1**.

consists of two halves of the $[Ni(mnt)_2]^-$ anion and one $[3CNBzTPP]^+$ cation. The Ni(III) ion of the $[Ni(mnt)_2]^-$ anion shows a square-planar coordination geometry. The Ni—S bond distances and the S—Ni—S bond angles (Table 2) within the five-membered rings agree well with those of [4CNBzTPP][Ni(mnt)$_2$] [24]. By comparing [3CNBzTPP][Ni(mnt)$_2$](**1**) with [4CNBzTPP][Ni(mnt)$_2$][24], some significant differences are found: (a) for the cation, the dihedral angles θ_1, θ_2, θ_3, and θ_4 between the C(14)—C(15)—P(1) reference plane and four phenyl rings are different, these angles for **1** are 97.5(θ_1)°, 156.4(θ_2)°, 88.5(θ_3)°, and 94.0(θ_4)° for the C(9)—C(14), C(16)—C(21), C(22)—C(27) and C(28)—C(33) rings respectively, while 86.3°, 89.8°, 43.9° and 124.8° for the latter; (2) the crystal system and space group are different, the former crystallizes in monoclinic lattice with $P2_1/n$ group, while the latter does in triclinic with P-1 group; (3) the stacking mode of the anions is different, the anions of [3CNBzTPP][Ni(mnt)$_2$](**1**) stack a column through Ni···S weak interactions with a Ni···S distance of 3.765 Å and the Ni(III) ions form a magnetic chain (Fig. 2a), while the anions of the latter form a dimer; (4) the overlapping mode of the anions in a column is different, the former is the Ni···S mode (Fig. 2b), while the latter is S···Ring mode [24]; (5) the weak interactions between the cations are different, there are two interactions in the $[3CNBzTPP]^+$ cations such as C—H···N hydrogen bond with a C(15)···N(5^{i}) (i = x + 1, y, z) distance of 3.384 Å and π···π stacking interaction with a distance of 3.551 Å between the phenyl rings (Fig. 2c). The $[3CNBzTPP]^+$ cation associate with the $[Ni(mnt)_2]^-$ anion *via* C—H···N weak interaction with the C(15)···N (1^{ii})(ii = $-x$ + 1/2, y −1/2, $-z$ + 1/2) distance of 3.369 Å. These weak interactions may play an important role in the stacking and stabilizing of the structure and result in the forming of a 3D network structure for **1** [Fig. 3].

As shown in Fig. 4a, the unit cell of **2** comprises a $[Ni(mnt)_2]^-$ anion and a $[3FBzTPPl]^+$ cation. The X-ray study reveals that when the 3-substituted group on the phenyl ring of benzyl group is changed from CN to F, some evident changes in crystal structure are found: (1) the crystal system changes from monoclinic for **1** to triclinic for **2**, and the space group changes from $P2_1/n$ to P-1; (2) the dihedral angles θ_1, θ_2, θ_3, and θ_4 change from 97.5°, 156.4°, 88.5° and 94.0° to 79.9°, 87.6°, 53.7° and 63.7°; (3) in a column of the anions (Fig. 4b), the overlapping mode of anions change from the Ni···S mode to the S···S and Ni···S modes [Figs. 5a and 5b], with the S···S and Ni···S distances of 3.681 Å and 3.654 Å; and the anions stack into a column through S···S and Ni···S interactions and the Ni(III) ions form a magnetic chain. In addition, the $[3CNBzTPP]^+$ cations form a dimer by C—H···F weak interaction with C(19)···F(1) distance of 3.371 Å (Fig. 5c). The packing diagram of **2** as viewed along a axis is shown in Fig. 5d, no obvious interactions were found between the anions and cations.

By comparing the structures of **1**, **2** and [4CNBzTPP][Ni(mnt)$_2$][24], when the position of substituted group on the phenyl ring of benzyl group from 4 to 3 or the 3-substituted group from CN to F, the dihedral angles θ_1, θ_2, θ_3 and θ_4 between the C—C—P reference plane and the phenyl rings, weak interactions, the stacking pattern of the cations and anions, and the overlapping mode of the anions are significantly changed. These evident changes in the crystal structure may further influence on the magnetic properties of these molecular solids.

3.2. Magnetic properties of *1* and *2*

The variable-temperature (2–300 K) magnetic data for **1** under an applied field of 2000 Oe, expressed as χ_m (emu mol^{-1}), are shown in Fig. 6a. As the temperature is lowered, the $\chi_m T$ value decreased from 0.305 emu K mol^{-1} at 300 K to 0.0256 emu K mol^{-1} at 2.0 K, indicative of an antiferromagnetic exchange. The magnetic susceptibility data in the temperature phase (50–300 K) of **1** can be finely fitted to the Curie–Weiss law with C = 0.352 emu K mol^{-1} and θ = −9.3 K (the red[1] solid line in inset of Fig. 6a).

As for **2**, when the temperature decreases, the value of $\chi_m T$ slightly decreases from 0.370 emu K mol^{-1} at 300 K to 0.0954 emu K mol^{-1} at 217 K, and as the sample is continuously

[1] For interpretation of color in Fig. 6, the reader is referred to the web version of this article.

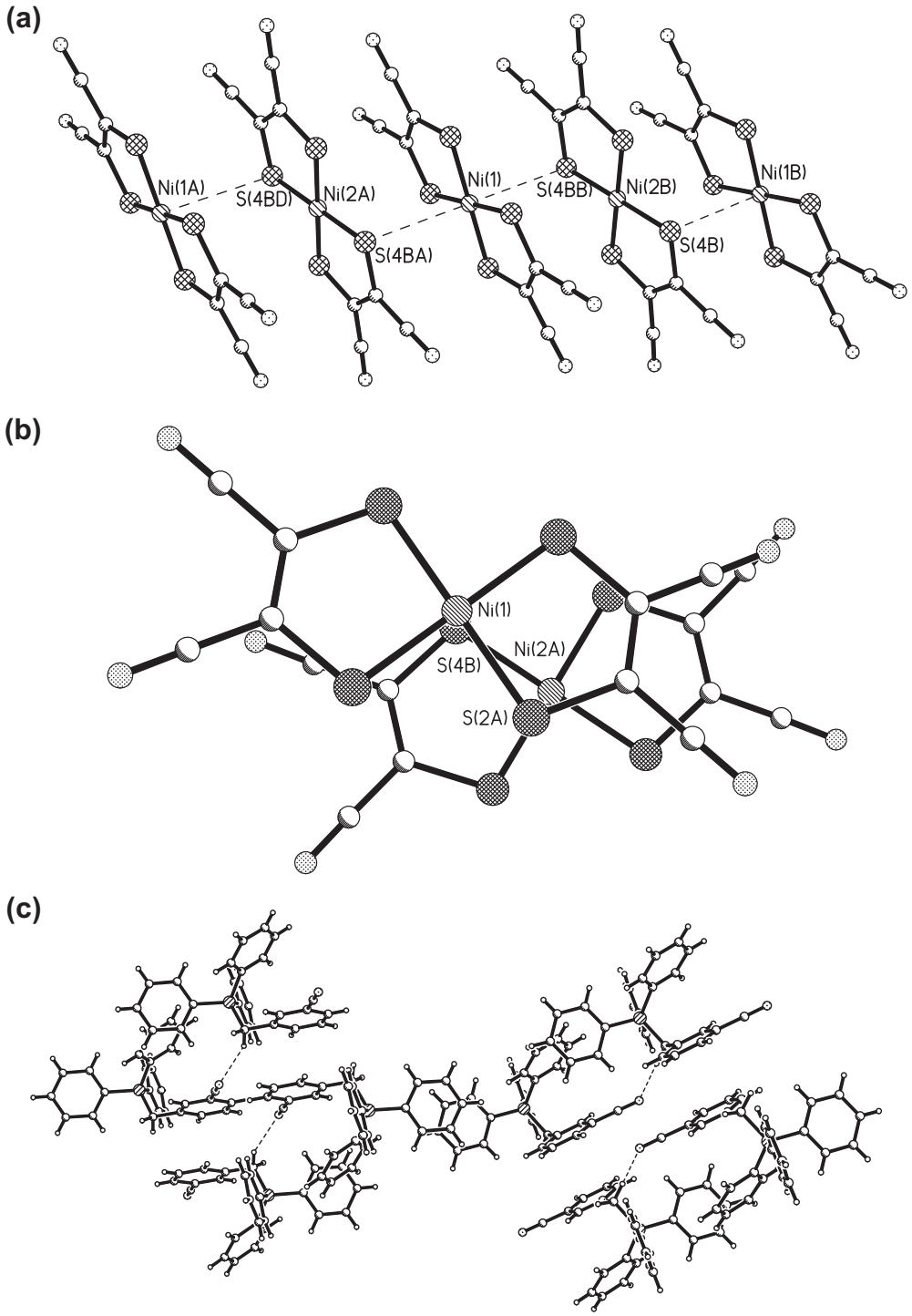

Fig. 2. (a) The column and 1D chain of the anions through weak Ni···S interactions between the anions for **1**. (b) The N···S overlapping mode of the anions for **1**. (c) The C—H···N hydrogen bonds and π···π stacking interactions between the cations for **1**.

cooled, the magnetic susceptibilities decrease exponentially (Fig. 6b), indicating that **2** shows the characteristics of a spin gap system [28–30]. The transition temperature is evaluated as the temperature at the maximum of the $d(\chi_m T)/dT$ derivative, that is, ~217 K for **2** (inset of Fig. 6b). The magnetic susceptibility from 2 to 225 K may be simulated by the formula [31]:

$$\chi_m = \alpha \exp(-\Delta/k_b T)/T + C/T + \chi_0$$

where α is a constant corresponding to the dispersion of excitation energy, Δ is the magnitude of the spin gap, k_b is the Boltzmann constant, C is a constant corresponding to the contribution of the magnetic impurity, χ_0 contributes from the core diamagnetism and the possible Van Vleck paramagnetism. A reasonable fit to the data within the range of 2–225 K for **2** is shown in Fig. 6b (the red solid line), and the corresponding parameters are given as follows: $\alpha = 3.96$, $\Delta/k_b = 945.04$ K, $\chi_0 = 3.0 \times 10^{-5}$ emu mol^{-1}, $C = 6.6 \times 10^{-4}$ emu K mol^{-1}, and $R = 5.0 \times 10^{-5}$ (R is defined as $\Sigma(\chi_m^{calcd} - \chi_m^{obsd})^2/(\chi_m^{obsd})^2)$). The magnetic coupling between $[Ni(mnt)_2]^-$ anions is very sensitive to the overlap fashion of neighboring $[Ni(mnt)_2]^-$ anions and intermolecular contacts [32], and the

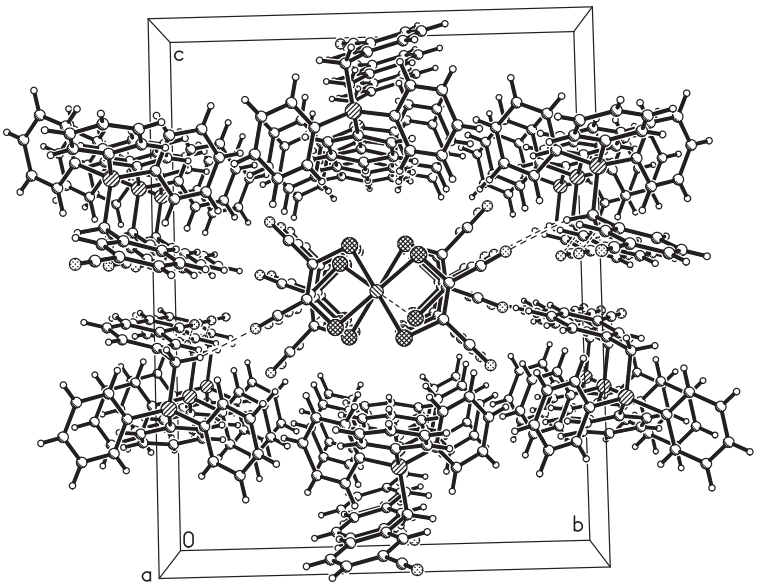

Fig. 3. Packing diagram of a unit cell for **1** as viewed along *a* axis.

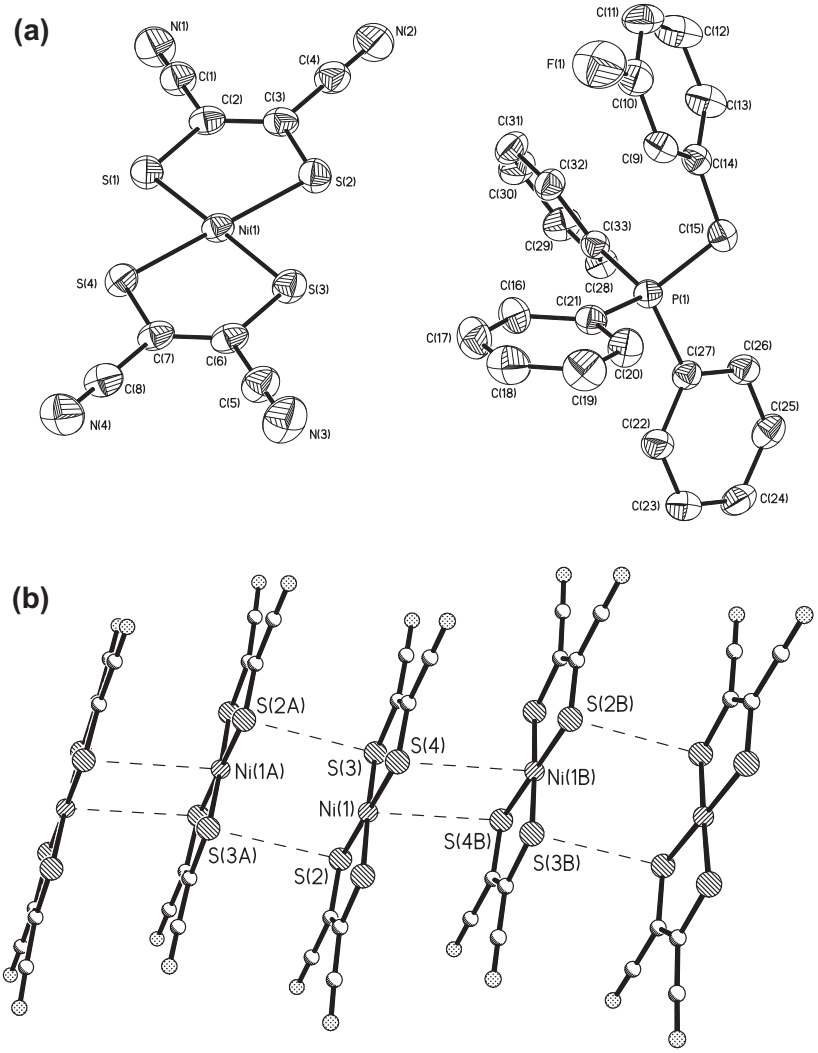

Fig. 4. (a) ORTEP plot (30% probability ellipsoids) showing the molecule structure for **2**. (b) The column and 1D chain of the anions through weak Ni···S and S···S interactions between the anions for **2**.

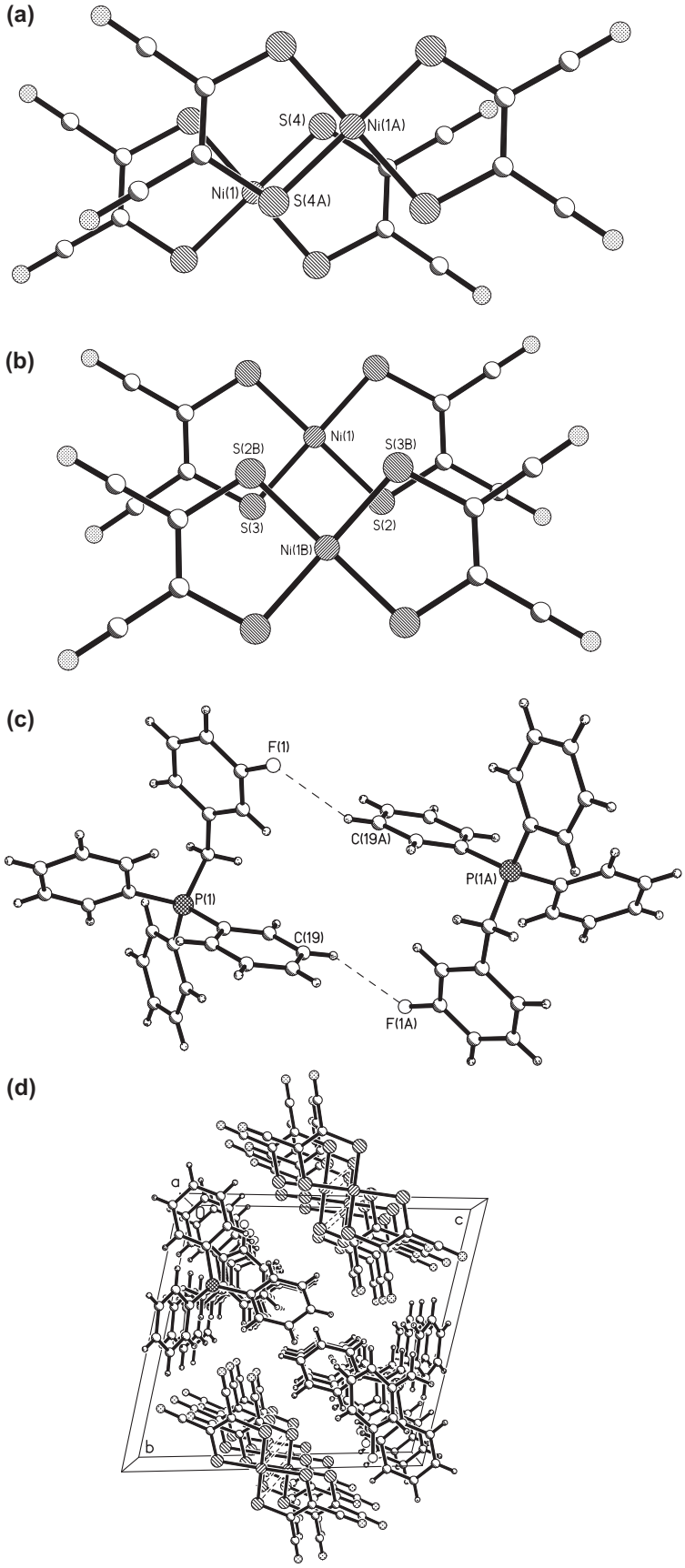

Fig. 5. (a) The Ni···S overlapping mode of the anions for **2**. (b) The S···S overlapping mode of the anions for **2.** (c) The C—H···F weak interactions between the cations for **2**. (d) Packing diagram of **2** as viewed along *a* axis.

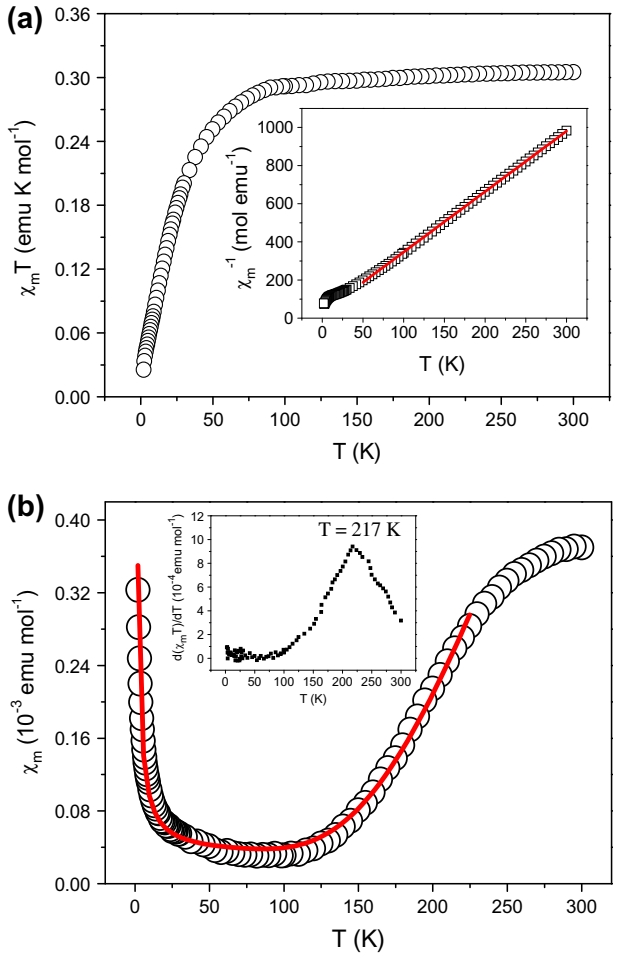

Fig. 6. (a) Plot of $\chi_m T$ *versus* T for **1** (inset: plot of χ_m^{-1} *versus* T)). (b) Plot of χ_m *versus* T for **2** (inset: plot of $d(\chi_m T)/dT$ *versus* T). The solid line is reproduced from the theoretic calculations and detailed fitting procedure described in the text).

magnetic exchange nature depends highly on the interplane distance (d) and the rotation angle (θ) [21]. Therefore, the difference between the magnetic behavior of **1**, **2** and [4CNBzTPP][Ni(mnt)$_2$] [24] may be understood. Compound **1** has a uniform column; the molecules are located on inversion centers, so the successive π···π interactions are equivalent. As a result, this compound **1** is paramagnetic. On the contrary, the molecules in compound **2** are located on general positions, so that the column is dimerized. The spin gap is the direct consequence for **2**. The spin-gap transition results from the magnetic exchange constant changing due to the non-uniform compression of the magnetic chain, the slippage of the [Ni(mnt)$_2$]$^-$ stack and the anisotropic contraction of the crystal on the temperature is lowered [33].

4. Conclusions

In conclusion, the crystal structures and magnetic properties were presented for two molecular materials, [3RBzTPP][Ni(mnt)$_2$] (mnt^{2-} = maleonitriledithiolate, [3RBzTPP]$^+$ = 3-R-benzyltriphenylphosphinium, R = CN(**1**), F(**2**)). The [Ni(mnt)$_2$]$^-$ anions of **1** and **2** stack into a column through the Ni···S or/and S···S interactions. The changes of the position or atom of the substituted group result in the changes of the weak interactions, the stacking pattern of the cations and anions, and the overlapping mode of the anions. These evident changes in the crystal structure may further result in the difference in magnetic properties, that is, **1** shows an antiferromagnetic coupling behavior, while **2** exhibits a spin-gap transition around 217 K.

Acknowledgements

This work has been partially supported by the key Academic Program of the 3rd phase "211 Project" of South China Agricultural University (No. 2009B010100001) and the Science and Technology Project (Nos. 2008B080701011, 2007B011000008) from Guangdong Science and Technology Department.

References

[1] T. Akutagawa, T. Motokizawa, K. Matsuura, S. Nishihara, S.I. Noro, T. Nakamura, J. Phys. Chem. 12 (2006) 5897.
[2] M.L. Mercuri, S. Curreli, P. Deplano, L. Pilia, A. Serpe, E.F. Trogu, J.A. Schlueter, E. Coronado, C.J. Gómez-García, J. Phys. IV, France 114 (2003) 425.
[3] N. Robertson, L. Cronin, Coord. Chem. Rev. 227 (2002) 93.
[4] L. Ouahab, Coord. Chem. Rev. 178–180 (1998) 1501.
[5] H. Nakajima, M. Katsuhara, M. Ashizawa, T. Kawamoto, T. Mori, Inorg. Chem. 43 (2004) 6075.
[6] K.L. Marshall, G. Painter, K.A. Lotito, A.G. Noto, P. Chang, Mol. Cryst. Liq. Cryst. 47 (2006) 449.
[7] P. Romaniello, F. Lelj, M. Arca, F.A. Devillanova, Theor. Chem. Acc. 117 (2007) 621.
[8] C.A.S. Hill, A. Charlton, A.E. Underhill, K.M.A. Malik, M.B. Hursthouse, A.I. Karaulov, S.N. Oliver, S.V. Kershaw, J. Chem. Soc. Dalton Trans. (1995) 587.
[9] P. Romaniello, F. Lelj, J. Mol. Struct.: Theochem. 636 (2003) 23.
[10] K. Wang, E.I. Stiefel, Science 291 (2001) 106.
[11] C.L. Ni, Q. Huang, H.R. Zuo, Y. Hou, Q.J. Meng, J. Coord. Chem. 62 (2009) 1502.
[12] C.H. Lin, C.G. Chen, M.L. Tsai, G.H. Lee, W.F. Liaw, Inorg. Chem. 47 (2008) 11435.
[13] K.M. Sung, R.H. Holm, J. Am. Chem. Soc. 124 (2002) 4312.
[14] A. Davison, N. Edelstein, R.H. Holm, A.H. Maki, Inorg. Chem. 3 (1964) 814.
[15] W.B. Pei, J.L. Liu, J.S. Wu, X.M. Ren, D.W. Gu, L.J. Shen, Q.J. Meng, J. Mol. Struct. 918 (2009) 160.
[16] M.G. Liu, C.L. Ni, C.J. Mao, J. Coord. Chem. 59 (2006) 1775.
[17] C.L. Ni, L.L. Yu, L.M. Yang, Inorg. Chim. Acta 359 (2006) 1383.
[18] J. Nishijo, E. Ogura, J. Yamaura, A. Miyazaki, T. Enoki, T. Takano, Y. Kuwatani, M. Iyoda, Solid State Commun. 116 (2000) 661.
[19] J.L. Xie, X.M. Ren, Y. Song, W.W. Zhang, W.L. Liu, C. He, Q.J. Meng, Chem. Commun. (2002) 2346.
[20] X.M. Ren, Q.J. Meng, Y. Song, C.S. Lu, C.J. Hu, Inorg. Chem. 41 (2002) 5686.
[21] Z.P. Ni, X.M. Ren, J. Ma, J.L. Xie, C.L. Ni, Z.D. Chen, Q.J. Meng, J. Am. Chem. Soc. 127 (2005) 14330.
[22] C.L. Ni, Y.Z. Li, Q.J. Meng, Coord. Chem. 9 (2005) 759.
[23] Y. Hou, J.R. Zhou, X.P. Liu, L.L. Yu, C.L. Ni, Trans. Met. Chem. 33 (2008) 411.
[24] J.R. Zhou, C.L. Ni, L.L. Yu, L.M. Yang, Inorg. Chim. Acta 361 (2008) 400.
[25] A. Davison, R.H. Holm, Inorg. Synth. 10 (1967) 8.
[26] S.B. Bulgarevich, D.V. Bren, D.Y. Movshovic, P. Finocchiaro, S. Failla, J. Mol. Struct. 317 (1994) 147.
[27] SHELXTL, Version 5.10. Structure Determination Software Programs, Bruker Analytical X-ray Systems, Inc., Madison, Wisconsin, USA, 2000.
[28] Y. Fujii, T. Goto, W. Fujita, K. Awaga, Physica B 329–333 (2003) 973.
[29] S. Nishihara, T. Akutagawa, T. Hasegawa, T. Nakamura, Chem. Commun. (2002) 408.
[30] C. Rovira, Chem. Eur. J. 6 (2000) 1723.
[31] L.C. Isett, D.M. Rosso, G.L. Bottger, Phys. Rev. B 22 (1980) 4739.
[32] A.T. Coomber, D. Beljonne, R.H. Friend, J.L. Brédas, A. Charlton, N. Robertson, A.E. Underhill, M. Kurmoo, P. Day, Nature 380 (1996) 144.
[33] X.M. Ren, S. Nishihara, T. Akutagawa, S. Noro, T. Nakamura, W. Fujita, K. Awaga, Chem. Phys. Lett. 418 (2006) 423.